Sensitive label-free biosensing using critical modes in aperiodic photonic structures

Svetlana V. Boriskina* **and Luca Dal Negro**

Department of Electrical and Computer Engineering, Boston University, Boston, MA, 20036, USA
**Corresponding author: sboriskina@gmail.com*

Abstract: In this paper, we introduce a novel approach for optical sensing based on the excitation of critically localized modes in two-dimensional deterministic aperiodic structures generated by a Rudin-Shapiro (RS) sequence. Based on a rigorous computational analysis, we demonstrate that RS photonic structures provide a large number of resonant modes better suited for sensing applications compared to traditional band-edge and defect-localized modes in periodic photonic structures. Finally, we show that enhanced sensitivity to refractive index variations as low as Δn=0.002 in RS structures results from the extended nature of critical modes and can enable the fabrication of novel label-free optical biosensors.

OCIS codes: (170.4580) Optical diagnostics for medicine; (130.6010) Sensors; (160.5298) Photonic crystals; (290.4210) Multiple scattering; (230.5750) Resonators; (170.4520) Optical confinement and manipulation.

References and links

1. S. Chan, P. M. Fauchet, Y. Li, L. J. Rothberg, and B. L. Miller, "Porous silicon microcavities for biosensing applications," Phys. Status Solidi A, **182**, 541–546 (2000).
2. B. Schmidt, V. Almeida, C. Manolatou, S. Preble, and M. Lipson, "Nanocavity in a silicon waveguide for ultrasensitive nanoparticle detection," Appl. Phys. Lett. **85**, 4854–4856 (2004).
3. S. Xiao and N. A. Mortensen, "Highly dispersive photonic band-gap-edge optofluidic biosensors," J. Eur. Opt. Soc. **1**, 06026 (2006).
4. N. A. Mortensen, S. Xiao, and J. Pedersen, "Liquid-infiltrated photonic crystals: enhanced light-matter interactions for lab-on-a-chip applications," Microfluidics and Nanofluidics 4, 117-127 (2008).
5. M. R. Lee and P. M. Fauchet, "Two-dimensional silicon photonic crystal based biosensing platform for protein detection," Opt. Express **15**, 4530–4535 (2007).
6. M. R. Lee and P. M. Fauchet, "Nanoscale microcavity sensor for single particle detection," Opt. Lett. **32**, 3284–3286 (2007).
7. E. Chow, A. Grot, L. W. Mirkarimi, M. Sigalas, and G. Girolami, "Ultracompact biochemical sensor built with two-dimensional photonic crystal microcavity," Opt. Lett. **29**, 1093–1095 (2004).
8. J. Scheuer, W. M. J. Green, G. A. DeRose, and A. Yariv, "InGaAsP annular Bragg lasers: theory, applications, and modal properties," IEEE J. Sel. Top. Quantum Electron. **11**, 476–484 (2005).
9. E. Krioukov, D. J. W. Klunder, A. Driessen, J. Greve, and C. Otto, "Sensor based on an integrated optical microcavity," Opt. Lett. **27**, 512–514 (2002).
10. F. Vollmer, S. Arnold, D. Braun, I. Teraoka, and A. Libchaber, "Multiplexed DNA quantification by spectroscopic shift of 2 microsphere cavities," Biophys. J. **85**, 1974–1979 (2003).
11. W. Fang, D. B. Buchholz, R. C. Bailey, J. T. Hupp, R. P. H. Chang, and H. Cao, "Detection of chemical species using ultraviolet microdisk lasers," Appl. Phys. Lett. **85**, 3666–3668 (2004).
12. K. De Vos, I. Bartolozzi, E. Schacht, P. Bienstman, and R. Baets, "Silicon-on-Insulator microring resonator for sensitive and label-free biosensing," Opt. Express **15**, 7610–7615 (2007).
13. I. M. White, H. Zhu, J. D. Suter, N. M. Hanumegowda, H. Oveys, M. Zourob, and X. Fan, "Refractometric sensors for lab-on-a-chip based on optical ring resonators," IEEE J. Sensors **7,** 28–35 (2007).
14. A. M. Armani, R. P. Kulkarni, S. E. Fraser, R. C. Flagan, and K. J. Vahala, "Label-free, single-molecule detection with optical microcavities," Science **317**, 783–787 (2007).
15. H. Zhu, I. M. White, J. D. Suter, P. S. Dale, and X. Fan, "Analysis of biomolecule detection with optofluidic ring resonator sensors," Opt. Express **15**, 9139–9146 (2007).
16. S. V. Boriskina, "Spectrally-engineered photonic molecules as optical sensors with enhanced sensitivity: a proposal and numerical analysis," J. Opt. Soc. Am. B **23**, 1565–1573 (2006).
17. A. D. McFarland and R. P. Van Duyne, "Single silver nanoparticles as real-time optical sensors with zeptomole sensitivity," Nano Lett. **3**, 1057–1062 (2003).

#97593 - $15.00 USD Received 18 Jun 2008; revised 28 Jul 2008; accepted 30 Jul 2008; published 4 Aug 2008

18. M. D. Malinsky, K. L. Kelly, G. C. Schatz, and R. P. Van Duyne, "Chain length dependence and sensing capabilities of the localized surface plasmon resonance of silver nanoparticles chemically modified with alkanethiol selfassembled monolayers," J. Am. Chem. Soc. **123**, 1471–1482 (2001).
19. C.-S. Cheng, Y.-Q. Chen, and C.-J. Lu, "Organic vapour sensing using localized surface plasmon resonance spectrum of metallic nanoparticles self assemble monolayer," Talanta **73**, 358–365 (2007).
20. I. M. White and X. Fan, "On the performance quantification of resonant refractive index sensors," Opt. Express **16**, 1020–1028 (2008).
21. S.G. Williams, ed., *Symbolic dynamics and its applications*, (American Mathematical Society, 2004).
22. M. R. Schroeder, *Number Theory in Science and Communication* (Springer-Verlag, 1985).
23. P. Prusinkiewicz and A. Lindenmayer, *The Algorithmic Beauty of Plants*, (Springer-Verlag, 1990).
24. J. M. Luck, "Cantor spectra and scaling of gap widths in deterministic aperiodic systems," Phys. Rev. B **39**, 5834–5849 (1989).
25. M. Queffélec, "Substitution dynamical systems-spectral analysis," in *Lecture Notes in Mathematics*, **1294** (Springer, 1987).
26. M. Dulea, M. Johansson, and R. Riklund, "Localization of electrons and electromagnetic waves in a deterministic aperiodic system," Phys. Rev. B, **45**, 105–114 (1992).
27. E. Macia, "The role of aperiodic order in science and technology," Rep. Prog. Phys. **69**, 397–441 (2006).
28. L. Dal Negro, C. J. Oton, Z. Gaburro, L. Pavesi, P. Johnson, A. Lagendijk, R. Righini, M. Colocci, and D. Wiersma, "Light transport through the band-edge states of Fibonacci quasicrystals," Phys. Rev. Lett. **90**, 055501 (2003).
29. L. Dal Negro, M. Stolfi, Y. Yi, J. Michel, X. Duan, L. C. Kimerling, J. LeBlanc, and J. Haavisto, "Photon bandgap properties and omnidirectional reflectance in Si/SiO_2 Thue-Morse quasicrystals," Appl. Phys. Lett. **84**, 5186–5188 (2004).
30. C. Rockstuhl, U. Peschel, and F. Lederer, "Correlation between single-cylinder properties and bandgap formation in photonic structures," Opt. Lett. **31**, 1741–1743 (2006).
31. L. Moretti and V. Mocella, "Two-dimensional photonic aperiodic crystals based on Thue-Morse sequence," Opt. Express, **15**, 15314–15323 (2007).
32. A. Della Villa, S. Enoch, G. Tayeb, F. Capolino, V. Pierro, and V. Galdi, "Localized modes in photonic quasicrystals with Penrose-type lattice," Opt. Express **14**, 10021–10027 (2006).
33. K. Mnaymneh and R. C. Gauthier, "Mode localization and band-gap formation in defect-free photonic quasicrystals," Opt. Express, **15**, 5089–5099 (2007).
34. Y. Lai, Z.-Q. Zhang, C.-H. Chan, and L. Tsang, "Anomalous properties of the band-edge states in large two-dimensional photonic quasicrystals," Phys. Rev. B **76**, 165132 (2007).
35. M. Notomi, H. Suzuki, T. Tamamura, and K. Edagawa, "Lasing action due to the two-dimensional quasiperiodicity of photonic quasicrystals with a Penrose lattice," Phys. Rev. Lett. **92**, 123906 (2004).
36. S. V. Boriskina, A. Gopinath, and L. Dal Negro, "Optical gaps, mode patterns and dipole radiation in two-dimensional aperiodic photonic structures," Physica E (in the press); preprint at http://arxiv.org/abs/0807.4131
37. L. Dal Negro, N.-N. Feng and A. Gopinath, "Electromagnetic coupling and plasmon localization in deterministic aperiodic arrays," J. Opt. A: Pure Appl. Opt. **10** 064013 (2008).
38. L. Kroon, E. Lennholm, and R. Riklund, "Localization-delocalization in aperiodic systems," Phys. Rev. B **66**, 094204 (2002).
39. L. Kroon and R. Riklund, "Absence of localization in a model with correlation measure as a random lattice," Phys. Rev. B, **69**, 094204 (2004).
40. G. Tayeb and D. Maystre, "Rigorous theoretical study of finite-size two-dimensional photonic crystals doped by microcavities," J. Opt. Soc. Am. A **14**, 3323–3332 (1997).
41. A. A. Asatryan, K. Busch, R. C. McPhedran, L. C. Botten, C. Martijn de Sterke, and N. A. Nicorovici, "Two-dimensional Green's function and local density of states in photonic crystals consisting of a finite number of cylinders of infinite length," Phys. Rev. E, **63**, 046612 (2001).
42. S. V. Pishko, P. Sewell, T. M. Benson, and S. V. Boriskina, "Efficient analysis and design of low-loss WG-mode coupled resonator optical waveguide bends," J. Lightwave Technol. **25**, 2487–2494 (2007).
43. Y. Wang, X. Hu, X. Xu, B. Cheng, and D. Zhang, "Localized modes in defect-free dodecagonal quasiperiodic photonic crystals," Phys. Rev. B **68**, 165106 (2003).
44. J. D. Joannopolous, S. Johnson, R. D. Meade, and J. N. Winn, *Photonic crystals: Molding the flow of light* (Princeton University, Princeton, 2008).
45. J. Vučković, M. Lončar, H. Mabuchi, and A. Scherer, "Design of photonic crystal microcavities for cavity QED," Phys. Rev. E **65**, 016608 (2001).
46. S. Blair and Y. Chen, "Resonant-enhanced evanescent-wave fluorescence biosensing with cylindrical optical cavities," Appl. Opt. **40**, 570–582 (2001).
47. A. Yamilov, X. Wu, X. Liu, R. P. H. Chang, and H. Cao, "Self-optimization of optical confinement in an ultraviolet photonic crystal slab laser," Phys. Rev. Lett. **96**, 083905 (2006).
48. S. V. Zhukovsky, D. N. Chigrin, and J. Kroha, "Low-loss resonant modes in deterministically aperiodic nanopillar waveguides," J. Opt. Soc. Am. B **23**, 2265–2272 (2006).

#97593 - $15.00 USD Received 18 Jun 2008; revised 28 Jul 2008; accepted 30 Jul 2008; published 4 Aug 2008

49. A. Sharkawy, D. Pustai, S. Shi, D. Prather, S. McBride, and P. Zanzucchi, "Modulating dispersion properties of low index photonic crystal structures using microfluidics," Opt. Express **13**, 2814–2827 (2005).
50. D. Erickson, T. Rockwood, T. Emery, A. Scherer, and D. Psaltis, "Nanofluidic tuning of photonic crystal circuits," Opt. Lett. **31**, 59–61 (2006).
51. R. W. Boyd and J. E. Heebner, "Sensitive disk resonator photonic biosensor," Appl. Opt. **40**, 5742–5747 (2001).
52. J. R. Lakowicz, J. Malicka, I. Gryczynski, Z. Gryczynski, and C. D. Geddes, "Radiative decay engineering: the role of photonic mode density in biotechnology," J. Phys. D: Appl. Phys. **36**, R240–R249 (2003).

1. Introduction

Periodic photonic crystals (PhCs) of different lattice symmetries with or without defects in one [1, 2] and two spatial dimensions [3-8] have recently been vigorously investigated for the fabrication of compact and sensitive biosensing platforms. Such sensors can detect the change in the refractive index of the ambient gas/liquid or the presence of infiltrated nanoparticles by monitoring the frequency shifts of high-quality factor (high-Q) optical resonances of the PhCs structures. Optical refractive index sensors offer the advantage of label-free technology, which significantly simplifies sample preparation while yielding real-time results. Alternative label-free optical biosensing platforms include microcavity-based structures such as optical microdisks, microrings, spheres, and toroids [9-16], as well as devices based on surface plasmon (SP) resonances in noble-metal nanoparticles and nanoparticles arrays [17-19]. The two major factors governing the efficiency and the detection limit (the smallest measurable refractive index change) of any of these optical sensor are: a) the magnitude of the wavelength shift in the resonant mode induced by the change in the ambient refractive index; b) the linewidth of the resonant mode, which determines the resolution in measuring such a shift [20]. The change of the refractive index can only be probed by the fraction of the resonant field that overlaps with the targeted analyte substances. It is therefore evident that an accurate balance between the resonant character of the sensing modes, measured by the quality factor Q, and their spatial localization (large field intensity in the sensing areas) must be achieved in order to improve the performances of label-free optical biosensors [20]. Biosensors based on high-index-contrast whispering-gallery (WG) mode microcavities demonstrate relatively low shifts of their modal frequencies, which are limited by the poor overlap of the mode evanescent field tails with the analyte. However, their performances greatly benefit from the ultra-narrow linewidths of the WG modes. On the other hand, SP sensors, which benefit from high values of field intensities in the detection region, are characterized by broad resonance linewidths (low Q-factors), which is a limiting factor in the spectral resolution of such devices.

In this context, the excitation of optical modes in aperiodic photonic structures may provide new exciting opportunities for the design of functional elements for bio-chemical sensing applications, as they offer different and largely unexplored possibilities to control and manipulate optical fields at the nanoscale. Deterministic aperiodic photonic structures share distinctive physical properties with both periodic media, i.e. the formation of well-defined energy gaps, and disordered random media, i.e. the presence of localized eigenstates with high field enhancement and Q-factors. However, unlike random media, deterministic aperiodic photonic structures are defined by the iterations of simple mathematical rules, rooted in symbolic dynamics [21], prime number theory [22] and L-system inflations [23], which can encode a fascinating complexity. In particular, photonic quasi-crystals and deterministic aperiodic structures can lead to novel design schemes for sensing devices based on the excitation of critically localized optical modes with unique transport properties [24, 25]. Critical modes are spatially localized field states characteristic of fractal and deterministic aperiodic environments that demonstrate fascinating scaling, spectral and localization properties [26]. In contrast the exponentially-localized Anderson modes in disordered media, critically localized states decay weaker than exponentially, most likely by a power law, and show a rich behavior with self-similar fluctuations extending across the structures [27]. The formation of photonic bandgaps and existence of critically-localized light states have already

#97593 - $15.00 USD Received 18 Jun 2008; revised 28 Jul 2008; accepted 30 Jul 2008; published 4 Aug 2008

been demonstrated in one-dimensional (1D) and two-dimensional (2D) aperiodic structures based on the Fibonacci, Thue-Morse and Penrose structures [28-33]. In particular, band-edge states in Fibonacci and Penrose quasi-periodic structures have been shown to be critically localized multi-fractal wavefunctions with anomalous transport properties, and their use for the fabrication of low-threshold compact lasers has been suggested [34, 35].

Recently, we have studied optical properties of the resonant modes of 2D aperiodic arrays of dielectric rods arranged according to different aperiodic sequences and have shown their high potential for engineering radiative rates and emission patterns of embedded sources [36]. However, to the best of our knowledge, a rigorous investigation of the potential of critical modes supported by aperiodic structures for sensing applications has not been reported to date. Our numerical simulations show that various types of 2D aperiodic (e.g. Thue-Morse) structures support critical modes featuring large frequency shifts with the change of the ambient refractive index, and therefore can potentially serve as biosensing platforms. However, in this paper we will limit the discussion to aperiodic photonic structures based on the 2D generalization of the non-periodic Rudin-Shapiro sequence [37], which is the most general example of a deterministic sequence with absolutely-continuous Fourier spectrum [26, 38], akin to random structures described by white spectra. In one spatial dimension, and within a two-letter alphabet, the RS sequence can simply be obtained by the iteration of the following inflation: AA→AAAB, AB → AABA, BA→BBAB, BB→BBBA. It is interesting to mention that even for one spatial dimension, there is presently no complete agreement on the localization character of the Rudin-Shapiro eigenmodes, although it has been recently pointed out that extended states coexist with exponentially-localized ones [38, 39]. As we have recently demonstrated, the RS sequence can be easily generalized into two spatial dimensions by a simple inflation method [37]. In this paper, we will discuss the photonic structures based on RS lattices of dielectric rods, and will theoretically demonstrate that they provide a large pool of high-Q critical modes with high sensitivity to the ambient refractive index change and thus can readily be used for label-free bio-sensing applications.

2. Computational method

Accurate and robust design of aperiodic photonic structures for specific application tasks is highly challenging. The lack of global translational symmetries in aperiodic structures renders conventional theoretical tools developed in the context of periodic photonic crystals (e.g., the plane wave expansion method) computationally intensive. To analyze in a uniform fashion both periodic photonic crystals and aperiodic photonic structures, we use a rigorous and highly efficient technique based on the generalized 2D Mie theory [40-42]. Electromagnetic field in the photonic structure composed of N_c cylindrical scatterers can be constructed as a superposition of partial fields scattered from each cylinder. These partial fields are expanded in infinite Fourier-Bessel series in the coordinate systems with the origins at the centers of individual cylinders. Using the addition theorem for Bessel functions, the interacting partial fields can be transformed into series expansions in the same coordinate system. Imposing the field continuity conditions at the boundary of each cylinder and truncating the infinite series at the maximum multipole order *N*, the final inhomogeneous matrix equation for the Lorenz/Mie multipole scattering coefficients can be obtained:

$$a_m^p - \sum_{l\neq p}\sum_{n=-N}^{N} S_m^p H_{m-n}^{(1)}\left(k\sqrt{\varepsilon_h}\, r_{pl}\right) e^{i(n-m)\theta_{pl}} a_n^l = S_m^p Q_m^p, \quad m=-N..N; \quad l,p=1..N_c \qquad (1)$$

Here, r_{pl} is the center-to-center distance between *p*-th and *l*-th cylinders; θ_{pl} is the argument of the vector $\vec{r}_{pl}=\vec{r}_l-\vec{r}_p$; $\varepsilon_h = n_h^2$ is the permittivity of the host medium; S_m^p are the polarization-dependent elements of the scattering matrix of each cylinder, which are obtained by applying the field boundary conditions at the cylinder cross-section contour; and Q_m^p are the Fourier expansion coefficients of the field illuminated by a line source in the host medium

#97593 - $15.00 USD Received 18 Jun 2008; revised 28 Jul 2008; accepted 30 Jul 2008; published 4 Aug 2008

(see e.g. [41, 42]). Eigenmodes of various photonic structures can be found by solving the homogeneous matrix Eq. (1). The computational effort required to solve the matrix equation is proportional to the number of cylinders, their separation distances, and the maximum multipolar order at which the infinite series were truncated. Although the computation time can be quite substantial when the structures are composed of many cylinders, which are either closely packed or widely separated, this technique produces essentially exact results provided that the series were truncated at a high enough multipolar order. The following simulations were performed with the relative accuracy better than 10^{-5}.

3. Results and discussion

In this section, we consider three types of photonic structures composed of dielectric cylinders in a low-index host medium as possible candidates for a sensitive and robust biosensing platform, and provide a theoretical comparison of their performance. These structures include: a periodic photonic crystal with a square lattice, the same PhC structure with a single localized defect (obtained by removing a central cylinder from the center of the lattice), and an aperiodic photonic structure based on a Rudin-Shapiro sequence. Dielectric cylinders in all the three lattices have the identical radii $r/a = 0.2$ (a is the nearest-neighbor center-to-center separation) and dielectric permittivity $\varepsilon = 10.5$. The material and structural parameters have been chosen to be the same as in Ref. 3 to provide comparison with the previously proposed optofluidic sensor based on the periodic PhC structure.

First, to study the optical modes spectra of each photonic structure, we calculate the total power radiated by a line source placed in its center by integrating the output energy flux through the closed contour L surrounding the structure [34, 42, 43] as follows:

$$P_{rad} = \oint_L \mathbf{S}(\mathbf{r}) \cdot \mathbf{n} dr \tag{2}$$

Here, $\mathbf{S}$ is the Poynting vector and $\mathbf{n}$ is a unit vector normal to the contour enclosing the structure. Existence of photonic bandgaps and spectral locations of resonant modes in photonic structures can be revealed by inspecting the frequency dependence of the total radiated energy flow. For finite-size photonic structures, bandgaps are manifested as regions of the reduced radiated power in their frequency spectra [34, 42, 43], while for infinite photonic lattices, radiation from the line source at the frequency inside the bandgap would have been completely suppressed. It is well-known that 2D photonic structures composed of dielectric cylinders feature spectral gaps for TM-polarized modes (electric field parallel to the cylinder axis), whose spectral positions are virtually independent from the arrangement of cylinders [30, 44].

In Fig. 1, we plot the radiation power spectra of the square-lattice periodic and RS structures in the vicinity of the first TM bandgap for smaller ($N_c \sim 30$, red lines) and larger structures ($N_c \sim 100$, blue lines). The total power radiated by the source embedded in a photonic structure is normalized by dividing it by the power radiated from the source in the free space. A clear difference can be observed in the behavior of the optical spectra of the two structure types with the increase of the sample size. For a periodic lattice, the size increase causes further reduction of the radiation power in the bandgap and also the shift of the band-edge modes, in accordance with previous studies [34]. A radiation power spectrum of the periodic PhC with a defect is also shown in Fig. 1(a). A single narrow peak appearing in the bandgap region corresponds to the excitation of a monopole defect mode (see e.g. [44]). Near-field distributions of the extended band-edge modes and a localized single-defect mode supported by the periodic structure are shown in Fig. 2. For comparison, a hexagonal lattice of 100 cylinders with the same material and geometrical parameters features a TM bandgap between $a/\lambda = 0.289$ and $a/\lambda = 0.467$.

#97593 - $15.00 USD Received 18 Jun 2008; revised 28 Jul 2008; accepted 30 Jul 2008; published 4 Aug 2008

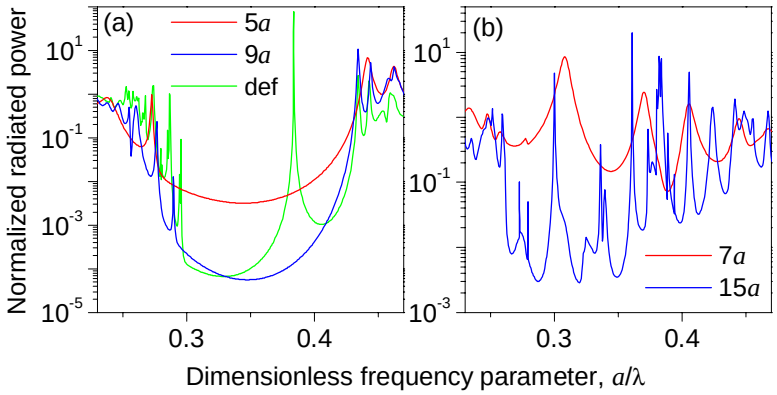

Fig. 1. The radiation power spectra of a TM-polarized line source located at the center of (a) periodic square lattice and (b) aperiodic Rudin-Shapiro lattice of dielectric cylinders (ε=10.5, r/a=0.2) in air. Two cluster sizes are considered for each configuration: (a) $5a\times5a$, N_c=36 (red) and $9a\times9a$, N_c=100 (blue); (b) $7a\times7a$, N_c=32 (red) and $15a\times15a$, N=120 (blue). The green line in Fig. 1(a) shows the radiation spectrum of the $10a\times10a$ (N_c=121) periodic structure with a single defect.

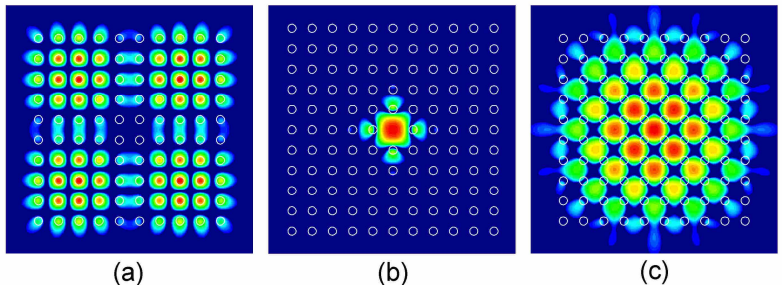

Fig. 2. Electric field intensity profiles of: (a) lower-frequency band-edge mode (a/λ=0.29, Q=2866.75, $\Delta\lambda(\Delta n$=0.002)=0.29 nm), (b) point-defect monopole mode (a/λ=0.384, Q=51037.2, $\Delta\lambda(\Delta n$=0.002)=1.82 nm), and (c) higher-frequency band-edge mode (a/λ=0.434, Q=341.46, $\Delta\lambda(\Delta n$=0.002)=1.8 nm) of the square-lattice periodic structure.

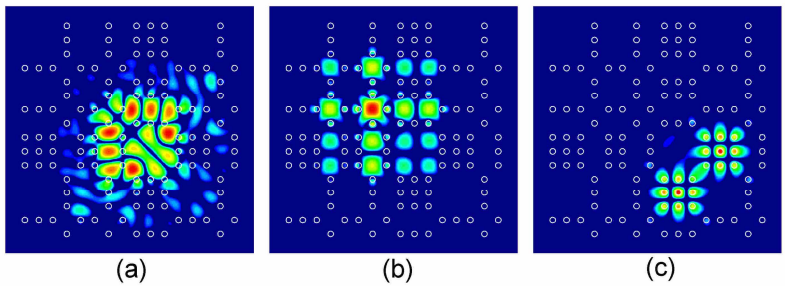

Fig. 3. Electric field intensity profiles of: (a,b) two critical modes (a/λ=0.443, Q=743.39, $\Delta\lambda(\Delta n$=0.002)=2.35 nm; a/λ=0.394, Q=6769.69, $\Delta\lambda(\Delta n$=0.002)=1.98 nm) and (c) a localized mode (a/λ=0.279, Q=1128.61, $\Delta\lambda(\Delta n$=0.002)=0.43 nm) of the RS aperiodic structure.

In sharp contrast to the above observations, the optical spectrum of the RS structure features multiple peaks inside the bandgap corresponding to the excitation of the localized and critical modes (see Fig. 1(b)). It can be clearly seen that with the increase of the structure size many additional peaks appear within the bandgap region, and their linewidths narrow

#97593 - $15.00 USD Received 18 Jun 2008; revised 28 Jul 2008; accepted 30 Jul 2008; published 4 Aug 2008

dramatically. Narrow linewidths translate into high Q-factors of optical modes and thus longer photon lifetimes. Typical near-field intensity portraits of three of the high-Q modes supported by the Rudin-Shapiro structure are plotted in Fig. 3. The mode shown in Fig. 3(c) is localized, and the intensity distributions shown in Fig. 3(a) and Fig. 3(b) correspond to critical modes, which extend across the structure with characteristic intensity fluctuations.

By comparing Figs. 1(a) and 1(b) we can conclude that the high-Q modes, which may be useful for lasing or sensing applications, are much more abundant in aperiodic photonic structures. We will now estimate the shifts of the resonant frequencies of these modes caused by the changes of the refractive index of the environment and compare them with the corresponding shifts of the modes of the periodic PhC. We assume that the volume of the analyte to be detected is large enough to cover the whole photonic structure, and thus it can be considered as an infinite homogeneous host medium in the following simulations. In Fig. 4(a), we plot the values of the red-shift ($\Delta\lambda = \lambda(n_h + \Delta n) - \lambda(n_h)$, nm) experienced by the optical modes of the larger-size ($N_c \sim 100$) square lattice periodic PhC (red bars) and the aperiodic RS structure (blue bars) scaled to operate at $\lambda \sim 1.55\,\mu\text{m}$ if the ambient refractive index is increased by $\Delta n = 0.002$. Figure 4(b) shows the quality factors of the corresponding modes. The chosen value of Δn represents the smallest increment that can be typically obtained in commercially available optical fluids and thus is often used to measure the sensitivity of PhC biosensors [3, 7]. Another useful figure of merit that is conventionally used to quantify the performance of optical biosensors is the refractive index sensitivity, defined as the ratio of the wavelength shift induced by the change of the ambient refractive index and the value of the index change: $S = \Delta\lambda / \Delta n_h$ (measured in nm/RIU).

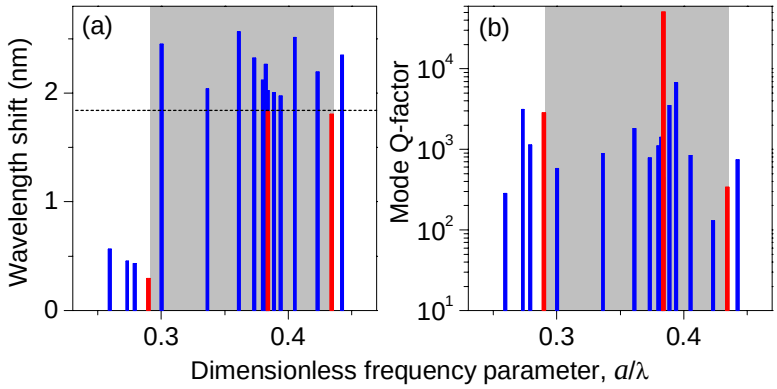

Fig. 4. (a). Shifts of resonant wavelengths of TM modes of the Rudin-Shapiro structure (blue) as well as the TM band-edge modes and a point-defect monopole mode of the periodic structure (red) with the change of the analyte refractive index by Δn=0.002; (b) Q-factors of the corresponding modes. The gray area indicates the band-gap of the periodic lattice. The dashed line shows the level of the largest wavelength shift achievable in the periodic structure.

It can be seen in Fig. 4(a) that the low-frequency band-edge mode (a so-called dielectric band [3, 4, 44]) of the periodic PhC shifts only slightly ($\Delta\lambda = 0.29\,\text{nm}$, S=147 nm/RIU), while the resonant frequencies of its high-frequency band-edge mode (an air(liquid) band [3, 4, 44]) and the defect mode demonstrate noticeable sensitivity to the refractive index change ($\Delta\lambda = 1.8\,\text{nm}$, S=902 nm/RIU and $\Delta\lambda = 1.82\,\text{nm}$, S=913 nm/RIU, respectively). This observation is in a perfect agreement with previous studies [3]; and such different behavior of the modes can be easily understood by inspecting the spatial distributions of their optical fields inside the periodic PhC lattice (see Fig. 2). Clearly, the modes that provide better

#97593 - $15.00 USD Received 18 Jun 2008; revised 28 Jul 2008; accepted 30 Jul 2008; published 4 Aug 2008

overlap of their electric field with the analyte show higher potential for sensing applications (see also [16, 20] for other examples of this effect). Band-edge modes of a hexagonal-lattice periodic PhC demonstrate a similar behavior: the low-frequency band-edge mode experiences a small wavelength shift of $\Delta\lambda = 0.28\,\text{nm}$ (S=138 nm/RIU), while the resonant frequency of the high-frequency band-edge mode is more sensitive to the ambient refractive index change ($\Delta\lambda = 1.44\,\text{nm}$, S=718 nm/RIU).

Likewise, long-wavelength modes appearing at or below the bandgap in the RS structure (either extended or localized like the mode shown in Fig. 3(c)) have electric field intensity mostly concentrated inside the dielectric cylinders, and thus interact with the analyte only via their evanescent field tails. Accordingly, they demonstrate small frequency shifts ($\Delta\lambda \sim 0.5\,\text{nm}$) caused by the change of the ambient refractive index (as seen in Fig. 4(a)). However, all the high-Q modes appearing in and just above the bandgap show enhanced sensitivity to the presence of the analyte over the modes of the periodic PhC ($1.98\,\text{nm} \le \Delta\lambda \le 2.56\,\text{nm}$ and $988\,\text{nm/RIU} \le S \le 1282\,\text{nm/RIU}$).

To quantify how the sensor refractive index sensitivity depends on the spatial distribution of the optical mode field, we introduce a parameter called the host medium filling fraction, i.e., the fraction of the optical mode energy that overlaps with the analyte [4, 15, 20]:

$$f_h = \frac{\int_{host} \varepsilon_h \left|E(\mathbf{r})\right|^2 dV}{\int \varepsilon(\mathbf{r})\left|E(\mathbf{r})\right|^2 dV}, \quad 0 \le f_h \le 1. \tag{3}$$

The integral in the numerator is taken only over the area covered by the analyte (outside the dielectric rods), while the one in the denominator is taken over the whole photonic structure. The dielectric filling fraction, i.e., the parameter that quantifies the relative overlap of the optical mode energy with the dielectric material of the rods, can be found via a very straightforward relation as follows: $f_d = 1 - f_h$ [4].

Other parameters that are frequently used to quantify the performance of microcavity-based devices are the effective optical mode volume V_{eff} and the normalized adimensional effective mode volume $\tilde{V}_{eff}$ (see, e.g., [45]):

$$V_{eff} = \frac{\int \varepsilon(\mathbf{r})\left|E(\mathbf{r})\right|^2 dV}{\varepsilon(\mathbf{r}_{\max})\left|E_{\max}\right|^2}, \; \tilde{V}_{eff} = V_{eff}\left(\frac{2n(\mathbf{r}_{\max})}{\lambda}\right)^2, \tag{4}$$

where $\mathbf{r}_{\max}$ is the position of the maximum field intensity.

In Fig. 5, we plot the values of the refractive index sensitivity of the periodic PhC bend-edge modes (red dots), single defect monopole mode (red diamond), and all the high-Q modes of the Rudin-Shapiro structure (blue dots) as a function of the host medium filling fraction (Fig. 5(a)) and of the normalized modal volume (Fig. 5(b)). The data shown in Fig. 5(a) confirm the intuitive conclusion that the increased overlap of the high-intensity portion of the modal field with the analyte improves the sensitivity of the device. Furthermore, the linear dependence of the mode refractive index sensitivity on the host medium filling fraction is clearly observed. This is in perfect agreement with the well-known expression for the spectral sensitivity obtained in the frame of the perturbation theory in the limit of small perturbations [4, 15, 20]:

$$S = f_h \cdot (\lambda / n_h). \tag{5}$$

The sensitivity values estimated by using (5) are plotted in Fig. 5(a) as a straight dashed line. On the contrary, the data presented in Fig. 5(b) show no correlation between the normalized effective volume and the refractive index sensitivity of the modes. In accordance with previous observations [45], resonant modes with optical fields localized in the low-index host

#97593 - $15.00 USD Received 18 Jun 2008; revised 28 Jul 2008; accepted 30 Jul 2008; published 4 Aug 2008

medium feature reduced $\tilde{V}_{eff}$ as compared to those of the modes with the high field intensity concentrated in the high-index dielectric material. However, no clear dependence of the mode sensitivity on the effective volume can be observed. We conclude that the normalized effective modal volume is not a useful parameter for estimating the sensitivity of the optical refractive index sensors. Nevertheless, it can still be considered a useful figure-of-merit for quantifying performance of optical biosensors based on other detection schemes, such as fluorescence enhancement [46] or a thermo-optic mechanism [14].

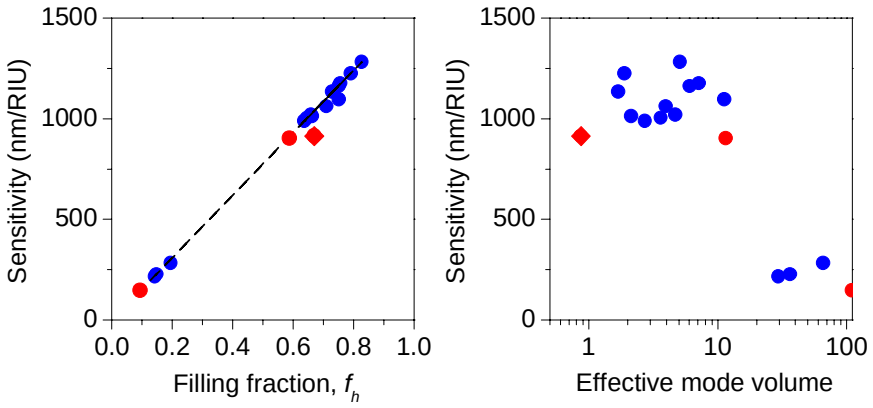

Fig. 5. Sensitivities of TM modes of the Rudin-Shapiro structure (blue circles), the TM band-edge modes (red circles), and a point-defect monopole mode (red diamond) of the periodic PhC as a function of (a) the filling fraction of the mode field energy in the host medium and (b) the normalized effective mode volume. Dashed line is obtained by using Eq. 5 for λ=1.55 μm.

It is also worth noting that the ability of aperiodic photonic structures to support many critical modes with high Q-factors and high sensitivities to the ambient refractive index change (Figs. 4 and 5) paves the way for using such structures as versatile sensor arrays. Note that the same structure with a fixed configuration can be used for sensing at different frequencies. Furthermore, our studies show that large aperiodic structures support high-Q critical modes that not only are characterized by different resonant frequencies but also have optical fields that are quasi-localized in different parts of the structure. As the mode frequency shift is caused only by the change of the refractive index in the area overlapping with the modal electric field, large aperiodic structures can be used as sensing arrays for simultaneous probing of different analytes at different operating frequencies.

High Q-factor of the mode is another crucial factor in achieving high sensitivity, as it is easier to detect shifts of narrow-linewidth resonances [20]. Note that although the point-defect mode in the 2D PhC demonstrates the highest in-plane Q-factor ($Q_{||} = 5.1 \cdot 10^4$), its overall Q-factor in a 3D realization ($1/Q = 1/Q_{||} + 1/Q_R$) will be severely limited by vertical out-of-plane loss (radiative Q-factor Q_R). This out-of-plane radiative loss results from the strong in-plane localization of the modal field, and one possible way of decreasing it is controllable delocalization of the in-plane modal field distribution, which in turn increases in-plane energy leakage [44]. Our investigation of localization properties of critical modes in aperiodic structures revealed the fact that the vertical and lateral leakage of their fields can be optimally balanced, which results in the optimization of the overall mode Q-factor. (Note that a similar effect has previously been observed in periodic photonic lattices with various degrees of structural and material disorder [47] and in 1-D aperiodic nanopillar waveguides [48]).

#97593 - $15.00 USD Received 18 Jun 2008; revised 28 Jul 2008; accepted 30 Jul 2008; published 4 Aug 2008

However, a detailed discussion of this phenomenon in 2-D aperiodic photonic structures is a subject of a separate study.

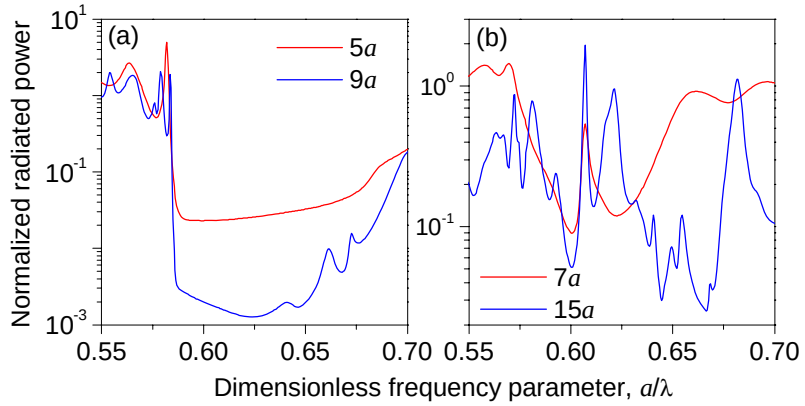

Fig. 6. The radiation power spectra of a TE-polarized line source located at the center of (a) periodic square lattice and (b) aperiodic Rudin-Shapiro lattice of dielectric cylinders (ε=10.5, r/a=0.2) in air. Two cluster sizes are considered for each configuration: (a) 5a×5a, N_c=36 (red) and 9a×9a, N_c=100 (blue); (b) 7a×7a, N_c=32 (red) and 15a×15a, N_c=120 (blue).

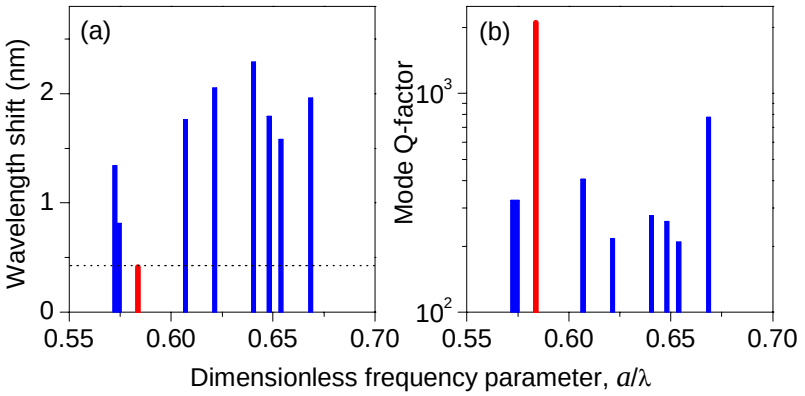

Fig. 7. (a). Shifts of resonant wavelengths of TE modes of the Rudin-Shapiro structure (blue) and a TE Bloch mode of the periodic structure (red) with the change of the analyte refractive index by Δn=0.002; (b) Q-factors of the corresponding modes. The dashed line shows the level of the largest wavelength shift achievable in the periodic structure.

We have also explored a possibility of using the TE-polarized modes (electric field in the array plane) of aperiodic structures for sensing applications. Normalized TE radiation power spectra of the periodic and RS lattices for two structure sizes ($N_c \sim 30$, red lines and $N_c \sim 100$, blue lines) are plotted in Fig. 6. No spectral gaps open for the TE-polarized waves [30, 44], however, the radiated power spectra of the RS structures feature a number of sharp variations with frequency. The peaks observed in Fig. 6(b) correspond to the critical modes, which may exist even in the absence of the optical bandgap owing to the spatial aperiodicity of the structure (compare to the previous observation of appearance of localized modes outside of the bandgap region in the Penrose photonic lattice of dielectric cylinders [32]). We calculated the resonant frequency shifts of these modes caused by the increase of the refractive index of the host medium by $\Delta n = 0.002$, and summarized the results in Fig. 7. As

#97593 - $15.00 USD Received 18 Jun 2008; revised 28 Jul 2008; accepted 30 Jul 2008; published 4 Aug 2008

in the case of the TM polarization, the corresponding data for the Bloch-type mode of a periodic structure are shown for comparison (red bars). The results presented in Fig. 7 clearly demonstrate that even in the absence of the TE bandgap aperiodic photonic structures sustain many quasi-localized critical modes that can be useful for sensing applications (wavelength shifts range from 1.34 nm (S=670 nm/RIU) to 2.29 nm (S=1145 nm/RIU)). Magnetic field distributions of the Bloch-type mode of the periodic structure and two critical modes of the Rudin-Shapiro structure are shown in Fig. 8.

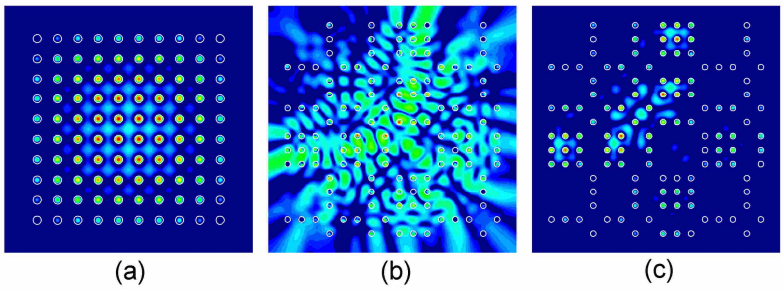

Fig. 8. Magnetic field intensity profiles of: (a) TE-polarized Bloch mode of the square-lattice periodic structure (a/λ=0.584, Q=2099.81, $\Delta\lambda(\Delta n$=0.002)=0.415 nm), and (b,c) two TE-polarized critical modes (a/λ=0.64, Q=275.28, $\Delta\lambda(\Delta n$=0.002)=2.29 nm; a/λ=0.575, Q=325.09, $\Delta\lambda(\Delta n$=0.002)=0.81 nm) of the Rudin-Shapiro aperiodic structure.

Finally, we would like to emphasize that the simulation results reported in this paper also predict that biosensors based on aperiodic photonic structures offer performance improvement over nanoparticle surface-plasmon biosensors. For example, the calculated wavelength shifts of the TM-polarized critical modes in Rudin-Shapiro structures scaled to operate at $\lambda \sim 600\,\text{nm}$ range from 0.76 nm to 0.99 nm (for $\Delta n = 0.002$), yielding refractive index sensitivity of 382-496 nm/RIU. Experimentally reported typical sensitivity values of surface-plasmon (SP) biosensors based on individual Ag nanoparticles and Ag nanoparticle arrays range from 150 to 235 nm/RIU for the same working frequency [17, 18]. Slightly higher sensitivity values (S=250 nm/RIU) have recently been reported for organic vapor SP resonance sensors based on the arrays of gold nanoshells [19]. It should also be noted that typical resonant peaks corresponding to the excitation of localized SP modes in noble-metal nanoparticles have much lower Q-factors than localized modes in photonic crystal cavities. As previously discussed, lower mode Q-factors (larger linewidths) result in the decrease of the spectral resolution of the sensor. Our results also compare very favorably with the data on the sensitivity values of several types of recently reported optical biosensors based on microdisks (S=22.89 nm/RIU, Q=4900), microrings (S=70 nm/RIU, Q=20,000) and point-defect microcavities in periodic photonic crystals (S=200 nm/RIU, Q=400) operating at $\lambda \sim 1.55\,\mu\text{m}$.

4. Conclusion

Through accurate numerical simulations, we have demonstrated a possibility of creating ultra-sensitive bio(chemical) sensors and sensor arrays based on aperiodic photonic structures. We predict resonant frequency shifts of critical modes in 2D Rudin-Shapiro structures composed of dielectric rods up to 2.56 nm for $\Delta n = 0.002$ and a working wavelength around 1.55 μm, which translates to the refractive index sensitivity of 1282 nm/RIU. For comparison, the high-frequency band-edge mode and the single-defect mode of a square-lattice periodic PhC with the same material properties and nearest-neighbor separations shift by 1.8 (S=902 nm/RIU) and 1.82 nm (S=913 nm/RIU), respectively (see also [3]). The observed high sensitivity of the spectral properties of aperiodic photonic structures to the ambient refractive index change provides a way of efficient dynamic manipulation of their optical spectra thus making them

#97593 - $15.00 USD Received 18 Jun 2008; revised 28 Jul 2008; accepted 30 Jul 2008; published 4 Aug 2008

ideal candidates for label-free optical biosensors and sensing substrates for opto-fluidic functional components [49, 50]. Finally, the high optical field intensity created at various pre-defined spatial and spectral positions in aperiodic photonic structures can be exploited in sensors based on different physical detection mechanisms, such as enhanced material absorption or fluorescence [46, 51, 52].

Acknowledgment

This work was partially supported by the Boston University College of Engineering Dean's Catalyst Award, the US Army Research Laboratory through the project: *Development of novel SERS substrates via rationally designed nanofabrication strategies*, the DARPA project: *Chemical Communication*, and the NATO Collaborative Linkage Grant CBP.NUKR.CLG 982430: *Micro- and nano-cavity structures for imaging, biosensing and novel materials.*

#97593 - $15.00 USD Received 18 Jun 2008; revised 28 Jul 2008; accepted 30 Jul 2008; published 4 Aug 2008